

Dryden Lectureship in Research

Parameter Estimation for Flight Vehicles

Kenneth W. Iliff*

NASA Ames Research Center, Edwards, California

The aircraft parameter estimation problem is used to illustrate the utility of parameter estimation, which applies to many engineering and scientific fields. Maximum-likelihood estimation has been used to extract stability and control derivatives from flight data for many years. This paper presents some of the basic concepts of aircraft parameter estimation and briefly surveys the literature in the field. The maximum-likelihood estimator is discussed, and the basic concepts of minimization and estimation are examined for a simple simulated aircraft example. The cost functions that are to be minimized during estimation are defined and discussed. Graphic representations of the cost functions are given to illustrate the minimization process. Finally, the basic concepts are generalized, and estimation from flight data is discussed. Some of the major conclusions for the simulated example are also developed for the analysis of flight data from the F-14 and Space Shuttle vehicles.

Nomenclature

A, B, C, D, F, G	= system matrices
C_l	= coefficient of rolling moment
C_m	= coefficient of pitching moment
C_n	= coefficient of yawing moment
$f(\cdot), g(\cdot)$	= general functions
GG^*	= measurement noise covariance matrix
H	= approximation to the information matrix
I_x, I_y, I_z, I_{xz}	= moment of inertia about subscripted axis, slug-ft ²
J	= cost function
L	= rolling moment divided by I_x , deg/s ² , or iteration number
L'	= rolling moment, ft-lb
L_{YJ}	= rolling moment due to yaw jet, ft-lb per jet
M	= Mach number
N	= number of time points or cases
n	= state noise vector, or number of unknowns
p	= roll rate, deg/s
\bar{q}	= dynamic pressure, lb/ft ²
Re	= Reynolds number
t	= time, s
u	= control input vector
V	= total velocity, ft/s
x	= state vector
z	= observation vector
\hat{z}	= predicted Kalman-filtered estimate
α	= angle of attack, deg
β	= angle of sideslip, deg
Δ	= time sample interval, s
δ	= control deflection, deg
η	= measurement noise vector
μ	= mean
ξ	= vector of unknowns
σ	= standard deviation
τ	= time, s
ϕ	= transition matrix, or bank angle, deg
ψ	= integral of transition matrix

Subscripts

p, α, β	= partial derivative with respect to subscripted variable
0	= bias, or at time zero
min	= minimum value

Superscripts

\sim	= predicted estimate
\wedge	= estimate
$*$	= transpose

Introduction

IT is difficult to present a topic as specialized as aircraft parameter estimation^{1,2} in a way that will interest a generalized audience of mathematicians, scientists, and engineers. The approach here is to portray parameter estimation as a specialized "curve-fitting" technique that can be applied to a broad class of problems. Much effort is expended in a variety of disciplines on a form of curve fitting, more specifically, the correlation of observed or inferred data with an assumed (though perhaps in a high- or infinite-dimensional space) mathematical model that is based on phenomenological considerations. This broad class of problems is referred to as system identification.

The application of system identification, sometimes referred to as the inverse problem (paraphrased as, "Given the answer, what is the question?"), presumably goes back to prehistoric times as humanity tried to master the environment by understanding, based on observation, certain phenomena (probably simple ones). Many of the physical laws stated by the Chinese, Egyptians, and Greeks were based on the same principles as are currently used in system identification. Through advancing technology and mathematical rigor, we can apply much more sophisticated techniques for making observations and for deducing the underlying phenomenology, but the basic problem of system identification remains the same.

For most physical systems, information about the general form of the system to be identified often can be derived from knowledge of the system. The most widely applied subfield of system identification is parameter identification, where the form of the mathematical model is assumed to be known. The model (an explicit function, a polynomial expansion, a look-up table, a finite-state machine defined for application of artificial intelligence, or many other forms) contains a finite number of parameters, the values of which need to be deduced or identified from the observations. One of the favored forms of the model for the most successful application is the state-space form (a rigorous treatment of state-space forms is given in Ref. 3). State-space models are very useful for dynamic

This article is an abridged version of the 1987 AIAA Dryden Research Lectureship, "Aircraft Parameter Estimation," presented as Paper 87-0623 at the AIAA 25th Aerospace Sciences Meeting, Reno, NV, Jan. 12-15, 1987; received March 21, 1988; revision received July 18, 1988. Copyright © 1987 American Institute of Aeronautics and Astronautics, Inc. No copyright is asserted in the United States under Title 17, U.S. Code. The U.S. Government has a royalty-free license to exercise all rights under the copyright claimed herein for Governmental purposes. All other rights are reserved by the copyright owner.

*Chief, Fluid and Flight Mechanics Branch, Dryden Flight Research Facility. Fellow AIAA.

systems in which responses are time functions. Autoregressive moving average (ARMA) models are also widely known; however, discrete-time ARMA models can readily be rewritten as linear state-space models,⁴ and so the discussion of state-space models presented in this paper is applicable to ARMA models.

An assumed model will not be an exact representation of the system no matter how carefully its form is selected. The experimental data will not be consistent with the assumed model for any parameter values. The model may be close but will not be exact, if only because the measurements or observations will be made with real, thus imperfect, sensors. Errors in observations and in the model need to be evaluated in determining the unknown parameters of the model and so the objective becomes the application of the "best" model (in some sense), instead of the correct model, to find the "best" estimates of the unknown parameters; this process is referred to as parameter estimation. The currently favored approach to parameter estimation, and the one discussed in this paper, is to minimize the error, in the least-squares sense, between the model response and the actual measured response; the estimates resulting in the minimum error are the best estimates. The theoretical formulation⁵ and application⁶ of the output error technique (which is a maximum-likelihood technique that is used throughout this paper) have been thoroughly documented.

Although the applications described in this paper pertain to aircraft, the techniques have been successfully applied in other fields where the mathematical model and observations are adequate. Parameter estimation may sound like one more arcane subject, but it has application in any field where observations must be made to agree with the assumed physics of a problem. There are many obvious applications in a variety of fields, such as spacecraft dynamics, gravitational perturbations, fluid dynamics and mechanics, optimal control, and guidance.

The application of the maximum-likelihood technique for parameter estimation of aircraft coefficients demonstrates a successful application of system identification technology. Analysts in the aircraft community accept and use system identification techniques on a routine basis. Although there are isolated problems (primarily in extending the application to more difficult flight regimes such as where the aircraft is dominated by poorly understood separated flow), there is little doubt that the basic application is highly successful. Contributing to this success is a well-understood, time-tested,^{7,8} physically derived model form that is reasonably representative of the true vehicle in most flight regimes; high-quality measurements of several relevant states; the ability to apply inputs specifically for system identification; and engineers familiar with system identification, aerodynamics, aircraft equations of motion, and the associated aerodynamic coefficients.

This paper first presents a brief survey of the contributions to system identification, and specifically aircraft parameter estimation, up to 1980, when the maximum-likelihood technique began to completely dominate the field. (References 6 and 9 give a broad view of contributions since 1980. Reference 9 is a bibliography of nearly 500 books, papers, and reports related to parameter estimation.) Some common uses of the estimated parameters are then discussed. The technique used for parameter estimation is then described, followed by an examination of the computational details and cost functions involved in error minimization. Finally, applications of the technique for improving high-performance aircraft and the Space Shuttle are described.

History of Parameter Estimation to 1980

General System Identification

The transition from hit-and-miss, rule-of-thumb system identification to mathematically sound approaches has been

gradual; certainly no single germinal work can be referenced. Gauss¹⁰ in 1809 discussed the inverse (system identification) problem and suggested some statistical approaches that are relevant even today. The discussion of Douglas¹¹ in 1940 and Gelfand and Levitan¹² in 1951 pertaining to the inverse problem certainly qualify as truly significant works contributing to the state of the art. The formulation by Feldbaum,¹³ one of the more significant works aimed at the current direction of investigation, is somewhat different than others discussed, but he did look at identification and control of the system as a single problem, the "dual-control" problem. During the 1960's, a plethora of publications was evidence of increased interest in problems of this type. Much of this interest was stimulated by the well-known early works of Kalman.

The bulk of general system identification theory and application up to 1980 has been summarized in several excellent survey papers.¹⁴⁻¹⁷

The system identification problem can be divided into two major subsets: deterministic (without state noise) and nondeterministic (with state noise). There are two classes of techniques for identification of nondeterministic systems: the Kalman filter (or more generally, the extended Kalman filter) technique, and the maximum-likelihood technique. Many precise applications do not truly fall into these classes, but they do tend to mimic one of the two techniques. The extended Kalman filter (discussed by Åström¹⁸ and Kashyap¹⁹) has been widely applied; however, this paper primarily examines the maximum-likelihood estimator, proposed by Balakrishnan²⁰⁻²² and developed in Refs. 23 and 24.

Aircraft Identification

In the following chronological survey of investigations that led to the development and widespread acceptance of the maximum-likelihood estimation technique for aircraft coefficient estimation, the more straightforward deterministic analysis is discussed first, followed by a brief discussion of nondeterministic analysis. Some of the investigations in estimation of unknown coefficients from aircraft dynamic response data are contained in Refs. 25 and 26. The National Advisory Committee on Aeronautics (NACA) had been publishing reports on stability derivatives (coefficients of the differential equations of motion) since the early 1920's. (The reports by Norton^{7,8} involved the identification of frequency and damping ratios from flight data.)

Deterministic Analysis

The sophistication and complexity of the methods used to estimate unknown coefficients from aircraft dynamic flight responses have increased over the past 40 years. In the late 1940's and early 1950's the frequency response methods (including steady-state oscillator analysis²⁷ and Fourier analysis²⁸) increased in popularity in aircraft analysis and in other applications. These methods yield the frequency response of the vehicle, but not the coefficients of the differential equations. Attempts were made to extract these coefficients by selecting values of the aircraft coefficients that resulted in the best fit of the frequency response.^{29,30} Regression techniques, such as linear least squares³¹ and weighted least-squares³⁰ techniques, were also applied to flight data at about that time. Unfortunately, regression techniques give poor results in the presence of measurement noise and yield biased estimates. The time vector technique³² has also been applied to flight data; however, it yields an incomplete set of coefficients, and the types of responses that can be analyzed are restricted to fairly simple motions. Analog matching techniques^{32,33} (time-consuming and somewhat tedious) have also been applied to flight data, but are limited because resulting estimates vary with the skill and technique of the operator. Comparisons of these early techniques^{34,35} showed that a more complete method of identification was needed.

In 1968, two independent studies^{36,37} of nonlinear minimization methods (output error methods) for obtaining aero-

dynamic coefficients were published, one describing the maximum-likelihood estimator^{36,38} (with a Gauss-Newton technique) to obtain a complete set of aerodynamic coefficients from flight data, and the other describing a quasilinearization technique^{37,39} to estimate some coefficients of an aircraft. One reason for the early success of these two methods is that previous research had furnished a well-defined model that adequately described the resulting motion of the vehicle. These two early results of aircraft identification by nonlinear minimization renewed interest in analysis of flight data. There was a later modification to these techniques to include a priori information.⁴⁰ The minimization of this modified cost functional does not result in a maximum-likelihood estimator because it is based on the joint probability distribution rather than the conditional probability. Other successful computer programs have been reported.⁴¹⁻⁴⁴ Extensive experience at many installations^{25,26,45-58} had been obtained using the maximum-likelihood estimator technique on dynamic flight responses.

Another approach, similar to these output error methods, was the application of the Kalman filter⁵⁹ to estimate the aerodynamic coefficients. Some of the early results obtained by the Kalman filter technique were unsatisfactory, i.e., the estimates of both the states and the parameters were biased and did not always converge to reasonable results. Improved results were obtained by adding the derivative of the state.⁶⁰ A weakness of the Kalman filter method is its dependence on the covariance matrix obtained from the filter.⁶⁰ However, a technique was developed for obtaining estimates of the covariance matrix with a suboptimal Kalman filter.⁵⁹ A successful application of the Kalman filter to provide the state estimates used for the estimation of stability and control derivatives and performance parameters was subsequently described.^{61,62}

Nondeterministic Analysis

As previously mentioned, two classes of techniques were offered for the estimation of systems with measurement and state noise: the Kalman filter (or more generally, the extended Kalman filter) technique^{18,19,59,60,63,64} and the maximum-likelihood technique.^{21-23,65,66} The maximum-likelihood estimator for the nondeterministic case is usually referred to as the filter error method.

The general application of the extended Kalman filter was discussed in Refs. 18 and 19. The extended Kalman filter for the discrete-time case was applied to simulated aircraft data with a state noise input.⁶⁰ A similar application⁶³ to aircraft flight response data gave inconclusive results because the state noise input was small, and the system was nonlinear. Somewhat better results were obtained with an application of a greatly simplified extended Kalman filter technique.⁶⁴

The maximum-likelihood estimator was applied to response data of an aircraft flying in atmospheric turbulence²³; the resulting coefficients were in agreement with results obtained for the same aircraft flying in smooth air, i.e., without state noise.

Most of the results presented in this paper are based on the output error method program⁶⁷; the Iliff-Maine code of this program is capable of using the Maine-Iliff formulation⁶⁸ (which can account for effects of state noise), although this feature is not used for the examples in this paper.

Basic Uses of Flight-Determined Coefficients

The extraction of unknown aerodynamic coefficients or stability and control derivatives from flight data has been of interest for many years.^{7,8} The coefficients are used to provide final verification of the predicted full-scale design, and to assist in the flight testing and verification of overall aircraft system performance.^{1,45} After the analysis of the flight test data, the aircraft coefficients can be compared with calculated coefficients, estimates from computational fluid dynamics, and wind-tunnel predictions, and these comparisons can be used to update prediction methods for the improvement of future

aircraft designs.^{1,46} Once an aircraft is built, the coefficients play an important role in the expansion of the flight test envelope.^{1,47} As estimates of the derivatives become available, they are used to upgrade fixed-based simulators to assist in flight planning and aircraft control system modification.^{1,48} In addition, the flight-determined coefficients can be used to establish compliance with the desired design specifications. Flight-determined coefficients are also used to establish the accuracy of airborne simulations⁴⁹ and to identify aircraft parameters for adaptive control.²³

Definition of Estimation Technique

The parameter estimation problem can be defined quite simply in general terms. The system under investigation is assumed to be modeled by a set of dynamic equations containing unknown parameters. To determine the values of the unknown parameters, the system is excited by a suitable input, and the input and actual system response are measured. The values of the unknown parameters are then inferred based on the requirement that the model response to the given input match the actual system response. When formulated in this manner, the unknown parameters can be identified easily by many methods; however, complicating factors arise when application to a real system is considered.

The first complication is the impossibility of obtaining perfect measurements of the response of any real system. The inevitable sensor errors are usually included as additive measurement noise in the dynamic model, and the theoretical nature of the problem then changes drastically. It becomes impossible to identify exactly the values of the unknown parameters; instead, the values must be estimated by some statistical criterion. The theory of estimation in the presence of measurement noise is relatively straightforward for a system with discrete-time observations, requiring only basic probability.

The second complication of real systems is the presence of state noise. State noise is random excitation of the system from unmeasured sources, the standard example for the aircraft stability and control problem being atmospheric turbulence. If state noise is present and measurement noise is neglected, the analysis results in the regression algorithm.⁶

When both state and measurement noise are considered,⁶⁸ the problem is more complex than in the cases that have only state noise or only measurement noise.

The final complication for real systems is modeling. It has been assumed throughout the discussion that for some value (called the best value) of the unknown parameter vector, the system is correctly described by the dynamic model. Physical systems are seldom described exactly by simple dynamic models, and so the question of modeling error arises. No comprehensive theory or modeling error is available. The most common approach is to ignore it; any modeling error is simply treated as state noise or measurement noise, or both, in spite of the fact that the modeling error may be deterministic rather than random. The assumed noise statistics can then be adjusted to include the contribution of the modeling error. This procedure is not rigorously justifiable, but combined with a carefully chosen model, it is probably the best approach available.

It is possible to make a more precise, mathematically probabilistic statement of the parameter estimation problem. The first step is to define the general system model (aircraft equations of motion), which can be written in the continuous-discrete form as

$$\dot{x}(t_0) = x_0 \quad (1)$$

$$\dot{x}(t) = f[x(t), u(t), \xi] + F(\xi)n(t) \quad (2)$$

$$z(t_i) = g[x(t_i), u(t_i), \xi] + G(\xi)\eta_i \quad (3)$$

where $\dot{}$ denotes derivative with respect to time. The state

noise vector is assumed to be zero-mean white Gaussian and stationary, and the measurement noise vector is assumed to be a sequence of independent Gaussian random variables with zero mean and identity covariance. For each possible estimate of the unknown parameters, a probability that the aircraft response time histories attain values near the observed values can then be defined. The maximum-likelihood estimates are defined as those that maximize this probability. Maximum-likelihood estimation has many desirable statistical characteristics; for example, it yields asymptotically unbiased, consistent, and efficient estimates.³⁸

If there is no state noise, then the maximum-likelihood estimator minimizes the cost function

$$J(\xi) = \frac{1}{2} \sum_{i=1}^N [z(t_i) - \tilde{z}_\xi(t_i)]^* (GG^*)^{-1} [z(t_i) - \tilde{z}_\xi(t_i)] + \frac{1}{2} N \ell_n |GG^*| \quad (4)$$

where $\tilde{z}_\xi(t_i)$ is the predicted response estimate of z at t_i for a given value of the unknown-parameter vector ξ . The cost function is a function of the difference between the measured and computed time histories.

If Eqs. (2) and (3) are linearized (as is the case for the stability and control derivatives in the aircraft problem),

$$\dot{x}(t_0) = x_0 \quad (5)$$

$$\dot{x}(t) = Ax(t) + Bu(t) + Fw(t) \quad (6)$$

$$z(t_i) = Cx(t_i) + Du(t_i) + G\eta_i \quad (7)$$

For the no-state-noise case, the $\tilde{z}_\xi(t_i)$ term of Eq. (4) can be approximated by

$$\tilde{x}_\xi(t_0) = x_0(\xi) \quad (8)$$

$$\tilde{x}_\xi(t_{i+1}) = \phi \tilde{x}_\xi(t_i) + \psi[u(t_i) + w(t_{i+1})]/2 \quad (9)$$

$$\tilde{z}_\xi(t_i) = C\tilde{x}_\xi(t_i) + Du(t_i) \quad (10)$$

where the transition matrix ϕ and the integral of the transition matrix ψ are given by

$$\phi = \exp[A(t_{i+1} - t_i)] \quad (11a)$$

$$\psi = \int_{t_i}^{t_{i+1}} \exp(A\tau) d\tau B \quad (11b)$$

When state noise is important, the estimator based on the nonlinear form of Eqs. (1-3) is intractable, and ad hoc techniques are required.⁶⁹

To minimize the cost function $J(\xi)$, we can apply the Newton-Raphson algorithm (or some other minimization technique), which chooses successive estimates of the vector of unknown coefficients ξ . If L is the iteration number, then the $L+1$ estimate of ξ is obtained from the L estimate as

$$\xi_{L+1} = \xi_L - [\nabla_\xi^2 J(\xi_L)]^{-1} [\nabla_\xi^* J(\xi_L)] \quad (12)$$

If $(GG^*)^{-1}$ is assumed fixed, the first and second gradients are defined as

$$\nabla_\xi J(\xi) = - \sum_{i=1}^N [z(t_i) - \tilde{z}_\xi(t_i)]^* (GG^*)^{-1} [\nabla_\xi \tilde{z}_\xi(t_i)] \quad (13)$$

$$\nabla_\xi^2 J(\xi) = \sum_{i=1}^N [\nabla_\xi \tilde{z}_\xi(t_i)]^* (GG^*)^{-1} [\nabla_\xi \tilde{z}_\xi(t_i)] - \sum_{i=1}^N [z(t_i) - \tilde{z}_\xi(t_i)]^* (GG^*)^{-1} [\nabla_\xi^2 \tilde{z}_\xi(t_i)] \quad (14a)$$

The Gauss-Newton approximation to the second gradient is

$$\nabla_\xi^2 J(\xi) \cong \sum_{i=1}^N [\nabla_\xi \tilde{z}_\xi(t_i)]^* (GG^*)^{-1} [\nabla_\xi \tilde{z}_\xi(t_i)] \quad (14b)$$

The Gauss-Newton approximation is computationally much easier than the Newton-Raphson method because the second gradient of the innovation never needs to be calculated. In addition, it can have the advantage of speeding the convergence of the algorithm, as is discussed in Ref. 6.

Figure 1 illustrates the maximum-likelihood estimation concept. The measured response is compared with the estimated response, and the difference between these responses is called the response error. The cost functions of Eqs. (4) and (11) include this response error. The minimization algorithm is used to find the coefficient values that minimize the cost function. Each iteration of this algorithm provides a new estimate of the unknown coefficients on the basis of the response error. These new estimates of the coefficients are then used to update values of the coefficients of the mathematical model, providing a new estimated response and, therefore, a new response error. The updating of the mathematical model continues iteratively until a convergence criterion is satisfied. The estimates resulting from this procedure are the maximum-likelihood estimates.

The maximum-likelihood estimator also provides a measure of the reliability of each estimate based on the information obtained from each dynamic maneuver. This measure of the reliability, analogous to the standard deviation, is called the Cramér-Rao bound,^{5,24} or the uncertainty level. The Cramér-Rao bound as computed by current programs should generally be used as a measure of relative accuracy rather than absolute accuracy. The bound is obtained from the approximation to the information matrix H , which is based on Eq. (14b); the actual information matrix is defined when evaluated at the correct values (not maximum-likelihood estimates) of all the coefficients. The bound for each unknown is the square root of the corresponding diagonal element of H^{-1} , i.e., for the i th unknown, the Cramér-Rao bound is $\sqrt{H^{-1}(i,i)}$.

The formulation and the minimization algorithm previously discussed [Eqs. (4-14)] are implemented with the Iliff-Maine code (MMLE3 maximum-likelihood estimation program). The program and computational algorithms are described fully in Ref. 67. All the computations shown and described in the remainder of this paper use the algorithms exactly as described in Ref. 67.

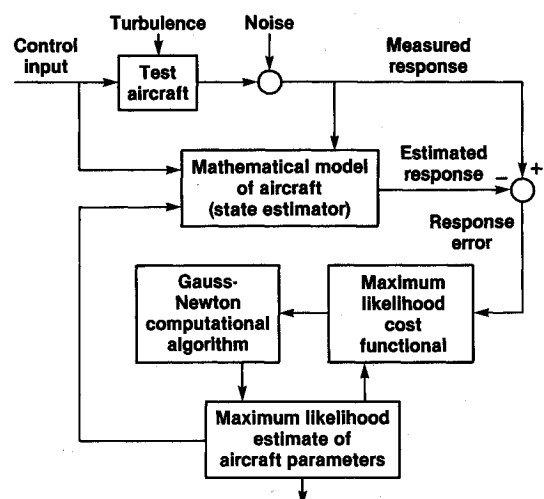


Fig. 1 Maximum-likelihood estimation concept.

Simple Simulated Example

For the discussion that follows, some knowledge of differential equations is assumed. A full derivation and a discussion of the aircraft equations of motion are given in Ref. 6.

The basic concepts involved in a parameter estimation problem will be illustrated by a simple simulated example representative of a realistic problem: an aircraft that exhibits pure rolling motion from an aileron input. This example, although simplified, typifies the motion exhibited by many aircraft in particular flight regimes, such as the F-14 aircraft flying at high dynamic pressure, the F-111 aircraft at moderate speed with the wing in the forward position, and the T-37 aircraft at low speed.

Derivation of an equation describing this motion is straightforward. Figure 2 illustrates an aircraft with the x axis perpendicular to the plane of the figure (positive forward on the aircraft). The rolling moment L' , roll rate p , and aileron deflection δ are positive as shown. For this example, the only state is p , and the only control is δ . The result of summing moments is

$$I_x \dot{p} = L'(p, \delta) \quad (15)$$

where I_x is the rolling moment about the subscripted (x) axis. The first-order Taylor expansion then becomes

$$\dot{p} = \frac{\partial L}{\partial p} dp + \frac{\partial L}{\partial \delta} d\delta \quad (16)$$

assuming small perturbations and using the notation

$$\dot{p} = L_p p + L_\delta \delta \quad (17)$$

where

$$L = L'/I_x$$

and the subscripts p and δ denote partial derivative with respect to the subscripted variable.

Equation (17) is a simple aircraft equation where forcing function is provided by the aileron and the damping by the damping-in-roll term L_p . In subsequent sections, we examine in detail the parameter estimation problem where Eq. (17) describes the system. For this single-degree-of-freedom problem, the maximum-likelihood estimator is used to estimate L_p or L_δ , or both, for a given simulated time history.

We will assume that the system has measurement noise, but no state noise; therefore, we can use Eqs. (1-3). Equation (4) then gives the cost function for maximum-likelihood estimation.

The weighting $(GG^*)^{-1}$ is unimportant for this problem, and so let $GG^* = 1$. For our example,

$$x_i = p_i \quad (18a)$$

$$z_i = x_i \quad (18b)$$

Therefore, Eq. (4) becomes

$$J(L_p, L_\delta) = \frac{1}{2} \sum_{i=1}^N [p_i - \tilde{p}_i(L_p, L_\delta)]^2 \quad (19)$$

where p_i is the value of the simulated measured response p at the time t_i , and $\tilde{p}_i(L_p, L_\delta)$ is the estimated time history of \tilde{p} at time t_i for $L_p = \hat{L}_p$ and $L_\delta = \hat{L}_\delta$. Throughout the rest of this paper where simulated data (not experimental flight data) are used, the simulated measured time history refers to p_i , and the estimated computed time history, which varies with each iteration, is $\tilde{p}_i(L_p, L_\delta)$. The estimated time history is a function of the current estimates of L_p and L_δ , but the simulated measured time history p_i is not.

The most straightforward method of obtaining \tilde{p}_i is with Eqs. (8) and (9). Using the previously stated notation,

$$\tilde{p}_{i+1} = \phi \tilde{p}_i + \psi(\delta_i + \delta_{i+1})/2 \quad (20)$$

where

$$\phi = \exp(L_p \Delta) \quad (21)$$

$$\psi = \int_0^\Delta \exp(L_p \tau) d\tau L_\delta = \frac{L_\delta [1 - \exp(L_p \Delta)]}{L_p} \quad (22)$$

and Δ is the length of the sample interval $t_{i+1} - t_i$.

The maximum-likelihood estimate is obtained by minimizing the cost function [Eq. (19)], which is done by applying the Gauss-Newton method. Equation (12) is used to determine successive values of the estimates of the unknowns during the minimization.

For this simple problem, $\xi = [\hat{L}_p \hat{L}_\delta]^*$, and successive values of \hat{L}_p and \hat{L}_δ are determined by updating Eq. (12). The first and second gradients of Eq. (12) are defined by Eqs. (13) and (14b).

We can now write the entire procedure for obtaining the maximum-likelihood estimates for this simple example. To start the algorithm, initial estimates of L_p and L_δ are needed to define the value ξ_0 . Using Eq. (12), ξ_1 and, subsequently, ξ_L are defined by using the first and second gradients of $J(L_p, L_\delta)$ from Eq. (19). The gradients for this particular example, from Eqs. (13) and (14b), are

$$\nabla_\xi J(\xi_L) = - \sum_{i=1}^N (p_i - \tilde{p}_i) \nabla_\xi \tilde{p}_i \quad (23)$$

$$\nabla_\xi^2 J(\xi_L) \cong \sum_{i=1}^N (\nabla_\xi \tilde{p}_i)^* \nabla_\xi \tilde{p}_i \quad (24)$$

Computational Details of Minimization

In the previous section, we specified the equations for a simple example and described the procedure for obtaining estimates of the unknowns from a dynamic maneuver. In this section, we give the computational details for obtaining the estimates. Some of the basic concepts of parameter estimation are best shown with simulated measured data, where the best (correct, in this simulated case) answers are known. Therefore, in this section we study an example involving simulated time histories. The example contains significant measured noise; consequently, the estimates are not the same as the correct values. The results are occasionally contrasted with the case with no measurement noise.

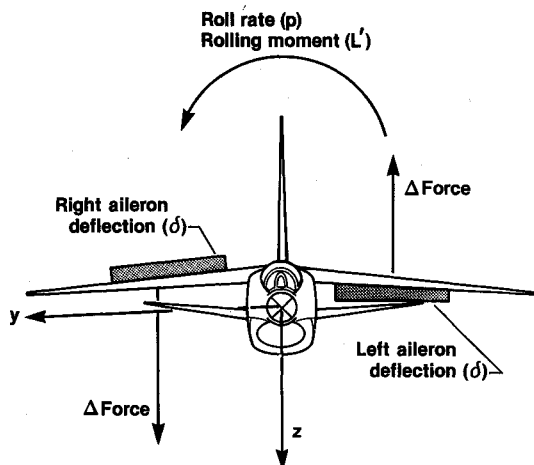


Fig. 2 Simplified aircraft nomenclature.

Table 1 Pertinent values as a function of iteration

L	$\hat{L}_p(L)$	$\hat{L}_\delta(L)$	$\phi(L)$	$\psi(L)$	J_L
0	-0.5000	15.00	0.9048	2.855	21.21
1	-0.3005	9.888	0.9417	1.919	0.5191
2	-0.2475	9.996	0.9517	1.951	5.083×10^{-4}
3	-0.2500	10.00	0.9512	1.951	1.540×10^{-9}
4	-0.2500	10.00	0.9512	1.951	1.060×10^{-14}

Table 2 Pertinent values as a function of iteration

L	$\hat{L}_p(L)$	$\hat{L}_\delta(L)$	$\phi(L)$	$\psi(L)$	J_L
0	-0.5000	15.00	0.9048	2.855	30.22
1	-0.3842	10.16	0.9260	1.956	3.497
2	-0.3518	10.23	0.9321	1.976	3.316
3	-0.3543	10.25	0.9316	1.978	3.316
4	-0.3542	10.24	0.9316	1.978	3.316
5	-0.3542	10.24	0.9316	1.978	3.316

For this simulated example, 10 points (time samples) are used. The simulated measured data, which we refer to as the measured data, are based on Eq. (17). The correct values are $L_p = -0.2500$ and $L_\delta = 10.0$ for the example. The input δ is used for the example, the sample interval $\Delta = 0.2$ s, and the initial conditions are zero. Tables of all the significant intermediate values of the calculations are given in Ref. 6. In the example, the initial values defining ξ_0 are $L_p = -0.5$ and $L_\delta = 15.0$.

The results of the parameter estimation analysis of the simulated measured time history for the case with no measurement noise are given in Table 1. The simulated measured data with pseudorandom Gaussian noise added to the roll rate are shown in Fig. 3. The signal-to-noise ratio is quite low in this example. The values of \hat{L}_p , \hat{L}_δ , ϕ , ψ , and J for each iteration are given in Table 2. The algorithm converges in four iterations. The behavior of the coefficients as they approach convergence is much like that in the no-noise case (Table 1). The most notable result of this case is that converged values of L_p and L_δ are somewhat different from the correct values.

In Fig. 4, the time history estimated using the correct values of L_p and L_δ is compared with that using the noisy estimates of L_p and L_δ . Because the algorithm converged to values somewhat different from the correct values, the two time histories are similar but not identical.

The accuracy of the converged elements can be assessed by looking at the Cramér-Rao inequality^{24,67} discussed previously. The Cramér-Rao bound can be obtained from an approximation to the information matrix H , where

$$H^{-1} = 2 J_{\min} \left\{ \sum_{i=1}^N [\nabla_{\xi} \tilde{z}_{\xi}(t_i)]^* (GG^*)^{-1} \nabla_{\xi} \tilde{z}_{\xi}(t_i) \right\}^{-1} / (N-1)$$

The Cramér-Rao bounds for L_p and L_δ are the square roots of the diagonal elements of the H^{-1} matrix, or $\sqrt{H^{-1}(1,1)}$ and $\sqrt{H^{-1}(2,2)}$, respectively. The Cramér-Rao bounds are 0.1593 and 1.116 for L_p and L_δ , respectively. The differences between \hat{L}_p and L_p and between \hat{L}_δ and L_δ are less than their respective bounds.

Cost Functions

In the previous section, we obtained the maximum-likelihood estimates for simulated time histories by minimizing the values of the cost functions. To fully understand what occurs in this minimization, we must study in more detail the form of the cost function and some of their more important characteristics. In this section, the cost function for the no-noise case is discussed briefly. The cost function for the noisy case is then discussed in more detail. The time histories studied in the

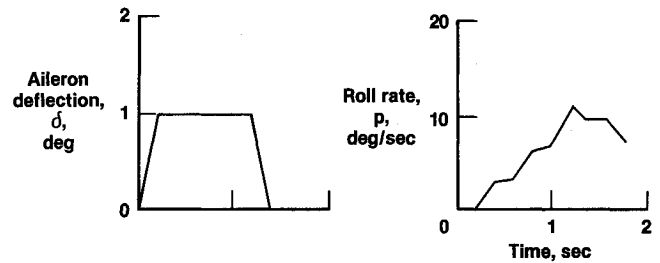


Fig. 3 Time history with measurement noise.

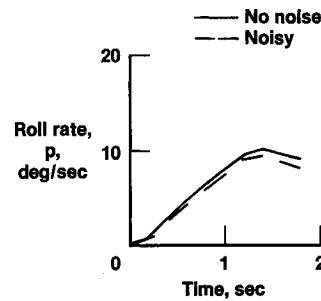


Fig. 4 Comparison of estimated roll rate from no-noise and noisy cases.

previous section are examined here. The noisy case is more interesting because it has a meaningful Cramér-Rao bound and is more representative of aircraft flight data.

It is important to remember that in this section everything related to cost functions [Eq. (19)] is based on simulated time histories that are defined by Eq. (17). For every measured time history we might choose (simulated or flight data), a complete cost function is defined. For the case of n variables, the cost function defines a hypersurface of $n+1$ dimensions. We could avoid bothering with the minimization algorithm if we could construct this surface and look for the minimum, but this is not a reasonable approach, because the number of variables is generally greater than two. Therefore, the cost function can be described mathematically, but not pictured graphically.

One-Dimensional Case

To illustrate the many aspects of cost functions, it is easiest to look first at cost functions having one variable. In an earlier section, the cost function of L_p and L_δ was minimized. That cost function is most interesting in the L_p direction. Therefore, the one-variable cost function studied here is $J(L_p)$, with the correct value of $L_\delta = 10.0$. Figure 5 (dashed line) shows the cost function plotted as a function of L_p for the no-noise case. As expected for this case, the minimum cost is zero and occurs at the correct value of $L_p = -0.2500$. It is apparent that the cost increases much more slowly for a more negative L_p than a positive L_p . In fact, the slope of the curve tends to become less negative where $L_p < -1.0$. Physically this makes sense because the more negative values of L_p represent cases of high damping, and the positive L_p represents an unstable system. Therefore, the \tilde{p}_i for positive L_p becomes increasingly different from the measured time history for small positive increments in L_p . For very large damping (very negative L_p), the system would show essentially no response. Therefore, further large increases in damping result in relatively small changes in the value of $J(L_p)$.

In Fig. 5 (solid line), the cost function based on the noisy case time history is plotted as a function of L_p . The correct L_p value (-0.2500) and the L_p value (-0.3218) at the minimum of the cost (3.335) are both indicated on the figure. The comments relating to the cost function based on the no-noise case also apply to the cost function based on the noisy case. Figure 5 shows clearly that the two cost functions are shaped

Table 3 Mean and standard deviations for estimates of L_p

Number of cases, N	Sample mean, $\mu(\hat{L}_p)$	Sample standard deviation, $\sigma(\hat{L}_p)$	Standard deviation of the sample mean $\sigma(\hat{L}_p)/\sqrt{N}$
5	-0.2668	0.0739	0.0336
10	-0.2511	0.0620	0.0196
20	-0.2452	0.0578	0.0129

Table 4 Estimates of L_p and Cramér-Rao bound as functions of the square root of noise power

Square root of noise power, G	Estimate of L_p	Cramér-Rao bound
0.0	-0.2500	—
0.01	-0.2507	0.00054
0.05	-0.2535	0.00271
0.10	-0.2570	0.00543
0.2	-0.2641	0.0109
0.4	-0.2783	0.0220
0.8	-0.3071	0.0457
1.0	-0.3218	0.0579
2.0	-0.3975	0.1248
5.0	-0.6519	0.3980
10.0	-1.195	1.279

similarly, but shifted in both the L_p and J directions. Only a small difference in the value of the cost would be expected far from the minimum because the "estimated" time history is so far from the simulated measured time history that it becomes irrelevant as to whether the simulated measured time history has noise added. Therefore, for large values of cost, the difference in the two cost functions should be small compared with the total cost.

The usefulness of the Cramér-Rao bound was discussed in the previous section. It is useful to digress briefly to discuss some of the ramifications of the Cramér-Rao bound for the one-dimensional case. The Cramér-Rao bound has meaning only for the noisy case. In the noisy example, the estimate of L_p is -0.3218 , and the Cramér-Rao bound is 0.0579 . The calculation of the Cramér-Rao bound was defined in the previous section for both the one-dimensional and the two-dimensional examples. The Cramér-Rao bound is an estimate of the standard deviation of the estimate. The scatter in the estimates of L_p should be of about the same magnitude as the estimate of the standard deviation. For the one-dimensional case discussed here, the range ($L_p = -0.3218$ plus or minus the Cramér-Rao bound, 0.0579) nearly includes the correct value $L_p = -0.2500$. If noisy cases are generated for many time histories (adding different measurement noise to each time history), then the sample mean and sample standard deviation of the estimates for these cases can be calculated. Table 3 gives the sample mean μ , sample standard deviation σ , and the standard deviation of the sample mean σ/\sqrt{N} , for 5, 10, and 20 cases. The sample mean, as expected, gets closer to the correct value of -0.2500 as the number of cases increases. This is also reflected in the table by the decreasing values of σ/\sqrt{N} , which are estimates of the error in the sample mean. The sample standard deviations indicate the approximate accuracy of the individual estimates. This standard deviation, which stays more or less constant, is approximately equal to the Cramér-Rao bound for the noisy case being studied here. In fact, the Cramér-Rao bounds of the 20 noisy cases used here (not shown in the table) do not change much from the values found for the particular noisy case being studied. Both of these results are in good agreement with the theoretical characteristics²⁴ of the Cramér-Rao bounds and maximum-likelihood estimators in general.

These examples indicate the value of obtaining more sample time histories (experiments or, in an aircraft example, dy-

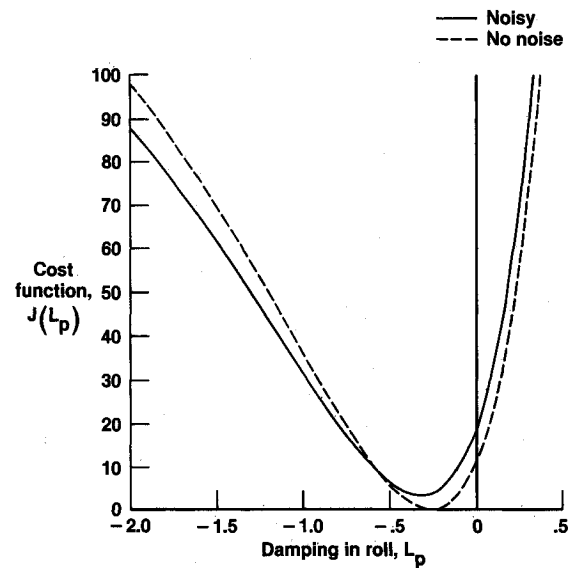


Fig. 5 Comparison of the cost functions for no-noise and noisy cases.

namic maneuvers). Having more samples improves confidence in the estimate of the unknowns. This also holds true in analyzing actual flight time histories (maneuvers); thus, it is always advisable to obtain data from several maneuvers at a given flight condition to improve the best estimate of each derivative.

The magnitudes of the Cramér-Rao bounds and of the error between the correct and estimated values of L_p are determined largely by the length of the time history and the amount of noise added to the correct time history. For the case being studied, it is apparent from Fig. 3 that a large amount of noise is added to the time history. The effect of the measurement noise power [GG^* , Eqs. (3) and (4)] on the estimate of L_p for the time history is indicated in Table 4. The estimate of L_p is much improved by decreasing the measurement noise power. A reduction in the value of G to one-tenth of the value in the noisy case being studied yields an acceptable estimate of L_p . For real experimental data, the measurement noise is reduced by improving the accuracy of the sensor outputs.

Two-Dimensional Case

In this section, the cost function dependent on both L_p and L_δ is studied. Even though the cost function is a function of only two unknowns, it is more difficult to visualize than is the one-dimensional case. The cost function over reasonable ranges of L_p and L_δ is shown in Fig. 6. The minimum must lie in the curving valley that gets broader toward the far side of the surface. The cost increases very rapidly in the region of positive L_p and large values of L_δ . The reason for this rapid increase is just an extension of the argument for positive L_p , given in the previous section. With this picture of the surface, we can look at the isoclines of constant cost on the L_p - L_δ plane (Fig. 7). The minimum of the cost function is inside the closed isocline. The steepness of the cost function in the positive L_p direction is once again apparent. The more nearly elliptical shape inside the closed isocline indicates that the cost is nearly quadratic there, so fairly rapid convergence in this

region would be expected. The L_p axis becomes an asymptote for cost as L_δ approaches zero. The cost is constant for $L_\delta = 0$ because no response would result from any aileron input; the estimated response is zero for all values of L_p , resulting in constant cost.

As in the one-dimensional case, the primary difference between the cost functions for the no-noise and noisy cases is a shift in the cost function (Fig. 5). In the one-dimensional case, the cost function for the noisy case was shifted so that the minimum was at a higher cost and a more negative value of L_p . In the two-dimensional case, the cost function exhibits a similar shift in both the L_p and the L_δ directions. The shift is small enough that the difference is not visible at the scale shown in Fig. 6. Figure 7 shows the isoclines of constant cost for the noisy case. The difference between the no-noise and noisy cases is a shift in L_p of about 0.1. Heuristically, one can see that this would hold true for cases with more than two unknowns; the primary difference between the two cost functions is near the minimum.

The next step is to examine the cost function near the minimum. Figure 8 shows the view of the cost function for the noisy case. The shape is roughly the same as it would be for

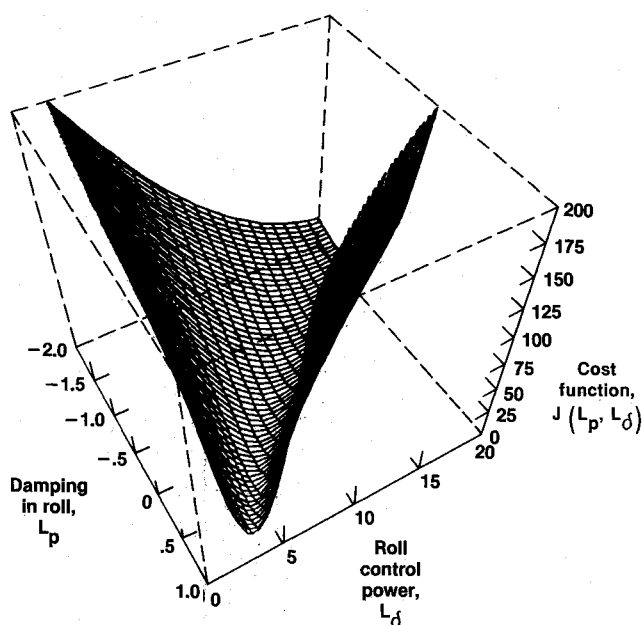


Fig. 6 Restricted view of cost function surface.

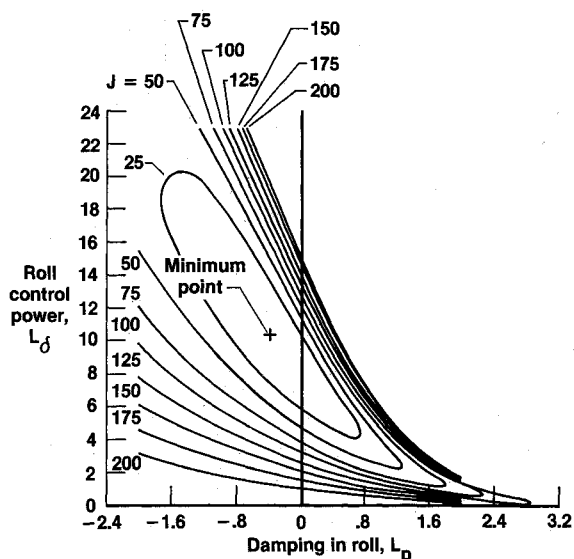


Fig. 7 Isoclines of constant cost in L_p and L_δ for noisy case.

the no-noise case, but the surface is shifted such that its minimum lies over $L_p = -0.3540$ and $L_\delta = 10.24$, and it is shifted upward to a cost function value of approximately 3.3.

To get a more precise idea of the cost function of the noisy case near the minimum, we must once again examine the isoclines. The isoclines in this region (Fig. 9) are much more like ellipses than those in Fig. 7. The results from Table 2 are included on Fig. 9, and so we can follow the path of the minimization example used before. The first iteration ($L = 1$) brought the values of L_p and L_δ very close to the values at the minimum, and the second essentially arrived at the minimum (viewed at this scale). One of the reasons the convergence is so rapid in this region is that the isoclines are nearly elliptical, demonstrating that the cost function is very nearly quadratic in this region. If we had started the Gauss-Newton algorithm at a point where the isoclines are much less elliptical (as in some of the border regions in Fig. 7), the convergence would have progressed more slowly initially, but it would have progressed at much the same rate as it entered the nearly quadratic region of the cost function.

Before concluding our examination of the two-dimensional case, we shall examine the Cramér-Rao bound. Figure 9 shows the uncertainty ellipsoid, which is based on the Cramér-Rao bound. (The relationships between the Cramér-Rao bound and the uncertainty ellipsoid are discussed in Ref. 5). The uncertainty ellipsoid almost encloses the correct values of L_p and L_δ . The Cramér-Rao bound for L_p and L_δ can be determined from the projection of the uncertainty ellipsoid onto the L_p and L_δ axes and then compared with the values calculated for the noisy case, which were 0.1593 and 1.116 for

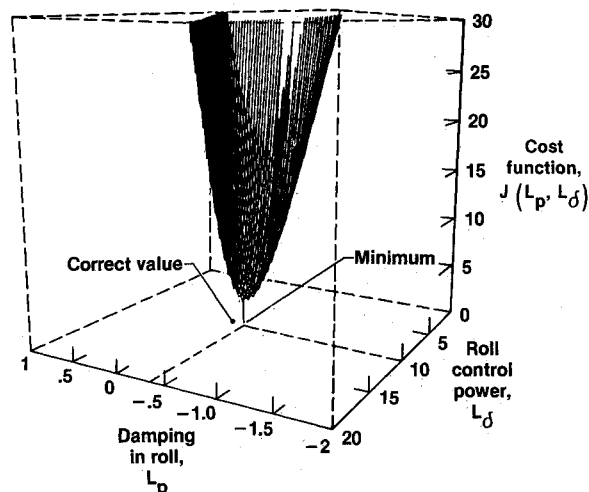


Fig. 8 Detailed view of cost function surface for noisy case.

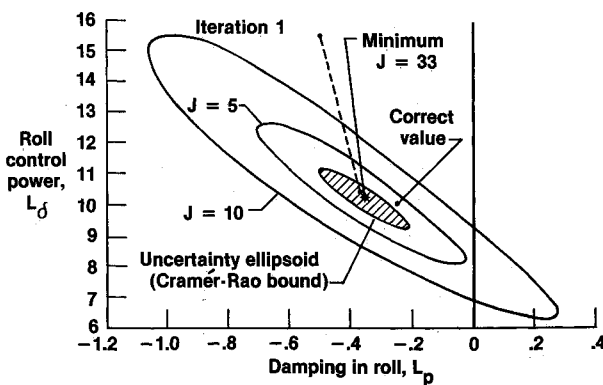


Fig. 9 Isoclines and uncertainty ellipsoid of the cost function for noisy case.

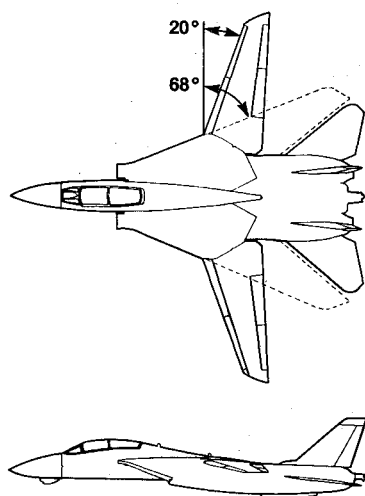


Fig. 10 F-14 airplane configuration.

L_p and L_δ , respectively. This projection is analogous to the case for n unknowns, but in that case the projection would be the $n + 1$ hyperellipsoid's projection onto a hypersurface.

Estimation Using Flight Data

We have examined the basic mechanics of obtaining maximum-likelihood estimates from simulated examples with one or two unknown parameters. To make the transition from theory to practical application, we present results obtained from analysis of actual flight data and discuss how the aircraft parameter estimation results are used to solve real problems. In this case, we illustrate the necessity of obtaining estimates of the aircraft coefficients of the differential equations of motion (the stability and control derivatives) to solve important and related problems encountered in flight. However, the aircraft stability and control example is only one of several applications of parameter estimation techniques; useful results can be obtained in many applications where the phenomenology is well understood. For the computationally difficult situation usually encountered with actual flight data, we obtain the maximum-likelihood estimates with the Liff-Maine code (MMLE3 program).⁶⁷ Before studying the specific examples, a brief historical review of some other uses of the estimates is presented.

In the past, the primary reason for estimating stability and control derivatives from flight tests was to make comparisons with wind-tunnel estimates. As aircraft became more complex, and as flight envelopes were expanded to include flight regimes that were not well understood, new requirements of the derivative estimates evolved. For many years, the flight-determined derivatives were used in simulations to aid in flight planning and in pilot training. The simulations were particularly important in research flight test programs in which an expansion of the envelope into new flight regimes was required. As more was learned about these new flight regimes, the complexity of the aircraft, and particularly their sophisticated flight control systems, increased. The design and refinement of the control system for these complex aircraft required higher-fidelity simulations. As a consequence, a more complete knowledge of the flight-determined stability and control derivatives was necessary. Almost all current high-performance aircraft have very complex control systems to compensate for their deficiencies in basic aerodynamic characteristics. Consequently, most flight test programs for these aircraft require a complete flight-determined set of stability and control derivatives, and parameter estimation techniques for estimating stability and control derivatives from flight data have become more sophisticated.

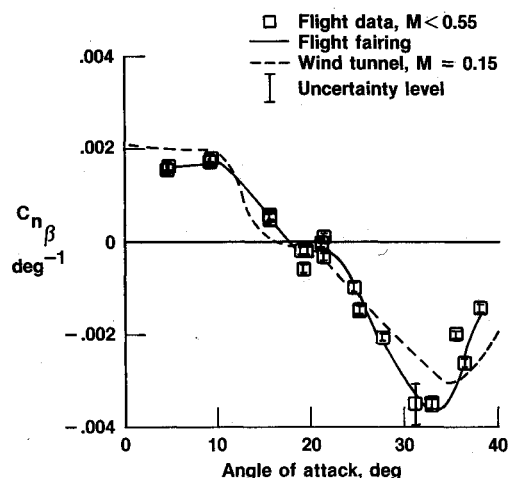


Fig. 11 Comparison of flight-derived estimates of static directional stability with wind-tunnel data.

At the Dryden Flight Research Facility of NASA's Ames Research Center (Ames-Dryden), analysts have been involved in the estimation of stability and control derivatives with maximum-likelihood estimators since 1966, and have successfully applied maximum-likelihood estimators to nearly 50 different aircraft configurations. Some of the experience gained through these applications is included in the bibliography of Ref. 9. Recent Ames-Dryden applications have concentrated on estimating stability and control derivatives to assist in designing or refining control systems. Two such applications (to be discussed in detail) are the F-14 and Space Shuttle programs. Both of these programs have made extensive use of high-fidelity, pilot-in-the-loop simulations, which are implemented using the best wind-tunnel data available. Portions of these flight test programs were defined to obtain data for refining simulator models.

The chosen method of enhancing the simulator model depends on the aircraft involved in the flight test program. The F-14 aircraft flew several flights specifically for defining the stability and control derivatives over a large-angle-of-attack range, because the necessary control refinement related to the high-angle-of-attack regime. The Space Shuttle entered from space on the most conservative trajectory to allow assessment of its characteristics before an envelope expansion was begun.

Once the flight data are obtained and analyzed, the simulator is updated to assist in control system design and further flight planning. Where flight results agree with wind-tunnel predictions, confidence in the simulation grows, and envelope expansion proceeds more efficiently.

The coefficients evaluated in this section are contained in the aircraft equations of motion, which are derived and discussed in detail in Ref. 6.

F-14 Aircraft

The F-14 aircraft is a twin-engine, high-performance fighter with variable wing sweep (Fig. 10). The Ames-Dryden F-14 program was intended to improve the handling qualities of the airplane at high angles of attack by incorporating several control system techniques.^{69,70} The first part of the program was dedicated to obtaining flight-determined stability and control derivatives for the subsonic envelope of the F-14 aircraft, the complete trimmed angle-of-attack range for Mach number $M \leq 0.9$.

In many instances the flight data agreed with the wind-tunnel predictions; Fig. 11 (from Ref. 69) shows the comparison of $C_{n\beta}$ (C_n being the coefficient of yawing moment) as a function of angle of attack α from flight- and wind-tunnel estimates. Throughout this and following discussions, a subscript to the coefficient denotes partial derivative with respect

to the subscripted variable. The symbols denote the estimate, and the vertical bar designates the uncertainty level (Cramér-Rao bound). the agreement is good, although there is some disagreement at $\alpha > 25$ deg; nevertheless, the same trends are seen for both flight- and wind-tunnel data.

Figure 12 shows the flight-determined C_{l_p} as a function of α for $M < 0.55$ and for $M = 0.9$. There was some uncertainty in the accuracy of the wind-tunnel predictions of C_{l_p} because the wind-tunnel model configuration was different from the flight configuration. The implementation of C_{l_p} at $M = 0.9$ in the simulation produced a previously unobserved wing-rock characteristic that had been observed in flight. The wing rock had been a troublesome characteristic, and its simulation was important in improving handling qualities through control system modifications. Figure 13 shows the flight-determined values of C_{l_β} as a function of α compared with the results of two different sets of wind-tunnel results. There had been some concern about the disagreement between the two sets of wind-tunnel results before flight. At low angles of attack, the three sets of estimates are in fair agreement; however, at $\alpha > 15$ deg, the flight data lie between the two sets of wind-tunnel data.

A last example from the F-14 aircraft shows how the wind tunnel and flight estimates interplay to improve a simulation. After the lateral-directional derivatives were incorporated in the simulation, the resulting simulated lateral-directional motions from a longitudinal-stick snap maneuver were found to be inconsistent with the flight response. Since the F-14

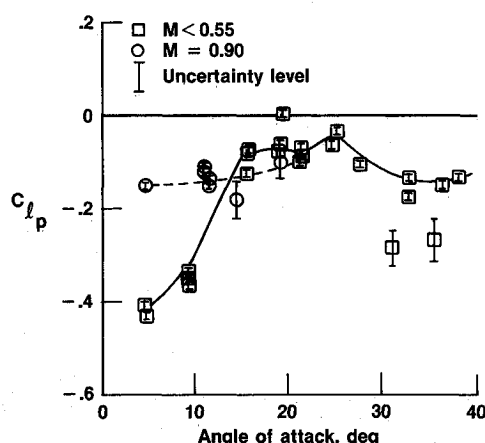


Fig. 12 Summary of flight-derived estimates of roll damping for $M < 0.55$ and $M = 0.9$.

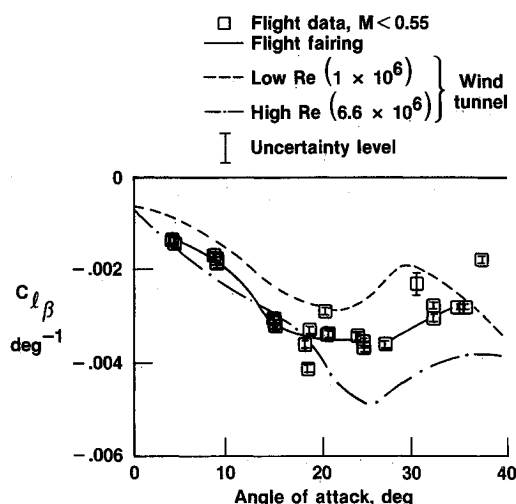


Fig. 13 Comparison of flight-derived estimates of dihedral effect with two sets of wind-tunnel data.

program was primarily a lateral-directional investigation, the longitudinal derivatives in the simulation had not been updated with the flight-determined values. When the flight-determined longitudinal derivatives were included in the simulation, the stick snap response agreed more closely with the flight response. In tracking down the inconsistency, a large discrepancy was discovered between the wind-tunnel and flight-determined values of C_{m_α} . This is shown in Fig. 14 where flight-determined C_{m_α} is compared with the wind-tunnel estimates of C_{m_α} for the untrimmed and trimmed conditions. Further investigation showed that the untrimmed values of C_{m_α} had been put in the simulation, and that the predicted trimmed values of C_{m_α} were in excellent agreement with flight estimates.

Examples using C_{l_p} , C_{l_β} , and C_{m_α} show how flight data, in addition to providing a primary source of estimates, can be used to help interpret wind-tunnel data; these data can then be used to improve the simulation at points away from steady-state flight data. Sometimes wind-tunnel data are available, but have been discounted or overlooked, and flight data can give new credence to these wind-tunnel data.

These F-14 flight data improved the simulation over a large part of the envelope. Since the F-14 high-angle-of-attack program also needed to examine responses of a highly transient nature, more tedious and time-consuming fine tuning of

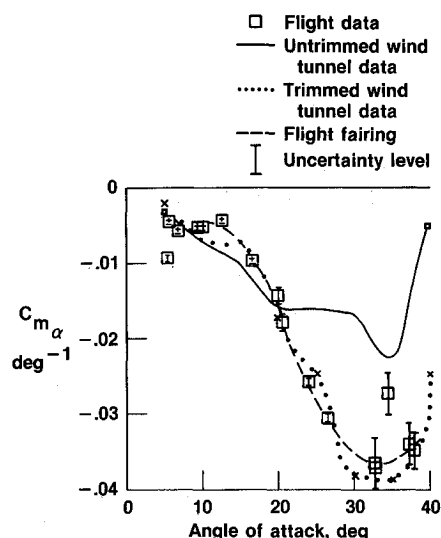


Fig. 14 Comparison of flight and wind-tunnel estimates for C_{m_α} .

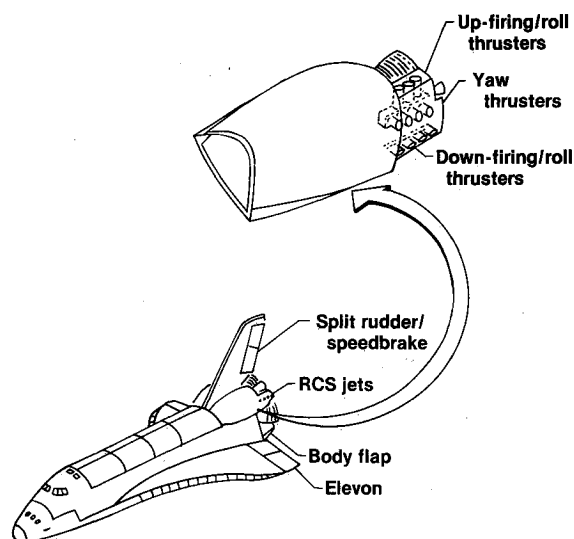


Fig. 15 Shuttle configuration.

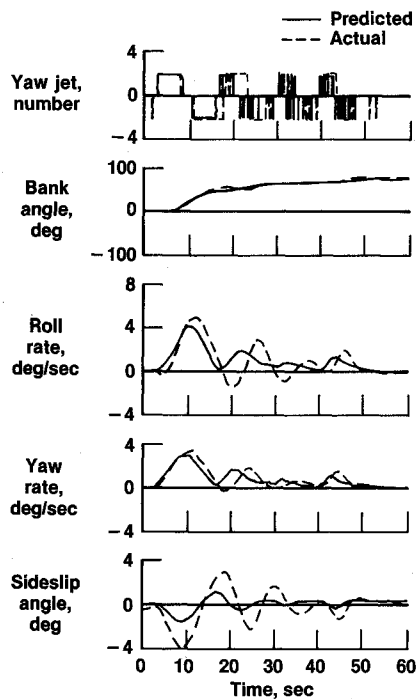


Fig. 16 Comparison of actual and predicted STS-1 bank maneuver at $M=24$.

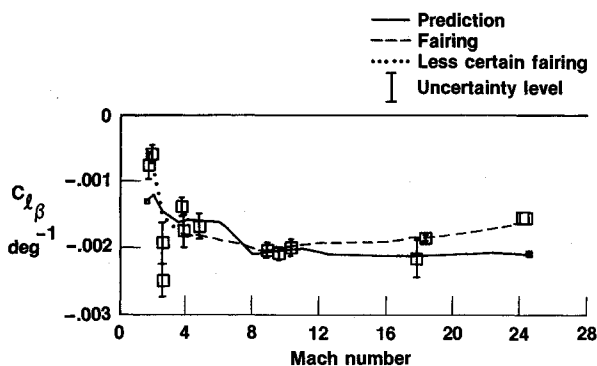


Fig. 17 Estimates of dihedral effect for the Space Shuttle.

the simulation was required for flight at other than near the trimmed conditions.⁷¹ With the resulting simulation, the proposed control system techniques were further refined; the result was a more efficient demonstration in flight.

This exemplifies the value of flight test parameter estimation in improving the handling qualities of an aircraft through control system improvements.

Space Shuttle Orbiter

The Space Shuttle Orbiter is a large double-delta-winged vehicle designed to enter the atmosphere and land horizontally. The entry control system consists of 12 vertical reaction control system (RCS) jets (6 up-firing and 6 down-firing) and 8 horizontal RCS jets (4 left-firing and 4 right-firing), 4 elevon surfaces, a body flap, and a split rudder surface (Fig. 15). The vertical jets and the elevons are used for both pitch and roll control. The jets and elevons are used symmetrically for pitch control and asymmetrically for roll control. More information on the configuration and flight plan is given in Ref. 72.

The F-14 example showed how parameter estimation can be used in an incremental flight test program, i.e., a progressive expansion of the flight envelope to obtain data in the more certain areas first and in the more challenging or hazardous ones later. However, the Space Shuttle program could not be approached in this manner, for the vehicle had to demonstrate on the first flight that it could be flown safely over most of its

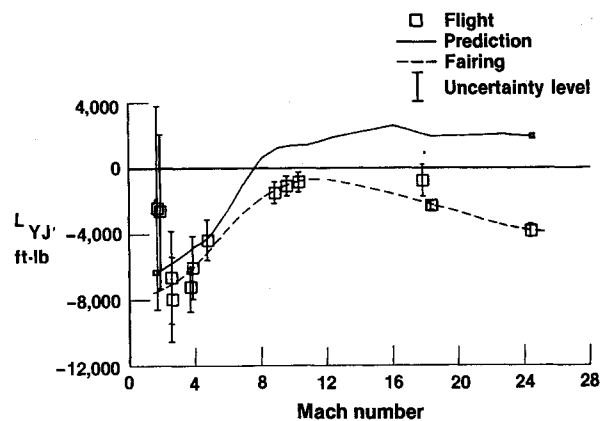


Fig. 18 Estimates of $L_{Y\dot{Y}}$ for the Space Shuttle.

envelope. Further complicating the program, this first flight included very hazardous flight regimes. The subsonic flight and landing characteristics had been demonstrated in the earlier approach and landing test program, but the hypersonic, peak heating, and transonic regions were largely unexplored for a vehicle of this type.

Extensive wind-tunnel tests were performed, and those data were incorporated into high-fidelity simulations. No matter how carefully wind-tunnel tests are performed, there are frequently discrepancies between the predictions and the demonstrated flight characteristics; therefore, uncertainties were defined for each stability and control derivative. These uncertainties (called variations in Ref. 73) were based to a large extent on previously reported discrepancies between predictions and flight.⁷⁴

In preparation for the first flight, a control system was developed to provide satisfactory closed-loop vehicle characteristics for derivatives that fell between the variations that had been previously defined. After flight data were obtained, the flight estimates of the stability and control derivatives were used to reduce the preflight variations. This reduction then allowed the control engineers to refine the control system and, therefore, to improve the Shuttle handling qualities. In addition, the flight-determined derivatives were used to determine if configuration placards (limitations on the flight envelope) could be modified or removed.

Some of the stability and control results obtained from the first three flights are contained in Refs. 75 and 76. One interesting example of where parameter estimation played an important role in the Shuttle program occurred during the first energy-management bank maneuver on the first entry of the Shuttle (STS-1). The response to the automated control inputs computed using the predicted stability and control derivatives is shown in Fig. 16 (solid line). It should be noted that the control inputs shown here (and for all other simulation comparisons) are the closed-loop commands from the Shuttle control laws. The maneuver was to be made at a velocity $V = 24,300$ ft/s and at a dynamic pressure $\bar{q} \approx 12$ lb/ft².

The actual STS-1 maneuver that occurred at this flight condition is also shown in Fig. 16 (dashed line), which depicts a more hazardous maneuver than was predicted. At this flight condition, the excursions must be kept small. The flight maneuver resulted in twice the angle-of-sideslip β peaks predicted and in a somewhat higher roll rate than predicted. Also, there was more yaw-jet firing than was predicted, and the motion was more poorly damped than predicted. It is obvious that comparing the predicted with the actual maneuver (Fig. 16) that the stability and control derivatives were significantly different than predicted. It is fortunate that the control system design philosophy discussed previously had been used for the Shuttle. Although the flight maneuver resulted in excursions greater than planned, the control system did manage to damp out the oscillation in less than 1 min.

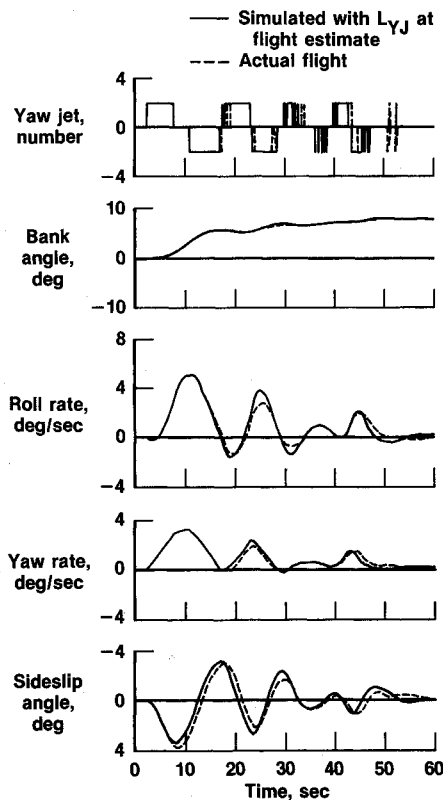


Fig. 19 Comparison of simulated bank maneuver with L_{YJ} at a flight-estimated value with the actual STS-1 bank maneuver.

With a less conservative design approach, the resulting entry maneuver could have been a good deal worse.

To assess the problem with the first bank maneuver, the flight-determined stability and control derivatives were compared with the predictions. Of all the derivatives obtained from STS-1, the two important ones that differed most from the predictions at the flight condition being discussed were $C_{l\beta}$ and the rolling moment due to yaw-jet firing L_{YJ} . Since the entry tends to monotonically decrease in Mach number, the derivatives can be best portrayed as functions of the guidance system "Mach number," which is $V/1000$. Figure 17 shows $C_{l\beta}$ as a function of guidance Mach number, and Fig. 18 shows L_{YJ} as a function of guidance Mach number. Only the estimates from STS-1 are shown in these figures.

When only the change in $C_{l\beta}$ was entered into the simulation data base, the maneuver looked very much like the original prediction; however, as expected, the frequency of the oscillations changed to be more representative of the actual flight frequencies. The effect on the simulation of changing only L_{YJ} from the predictions is shown, with the flight response, in Fig. 19. These two time histories are very close, considering that the other differences between the flight-determined and predicted derivatives have been ignored.

It is apparent that the primary problem with the initial bank maneuver was the poor prediction of L_{YJ} . The control system software is very complex, and it cannot be changed and verified between Shuttle missions; therefore, an interim approach was taken to keep this large excursion from occurring on future flights. The flight-determined derivatives were put into the simulation data base, and the Shuttle pilots practiced performing the maneuver manually, trying to attain a smaller response within more desirable limits. The maneuver was performed manually on STS-2 to STS-4. Figure 20 shows the manually flown maneuver from STS-2. For this maneuver, roll rate, yaw rate, and sideslip angle were within the desired limits. The maneuver does not look like the original predicted response because the derivatives and the input were different,

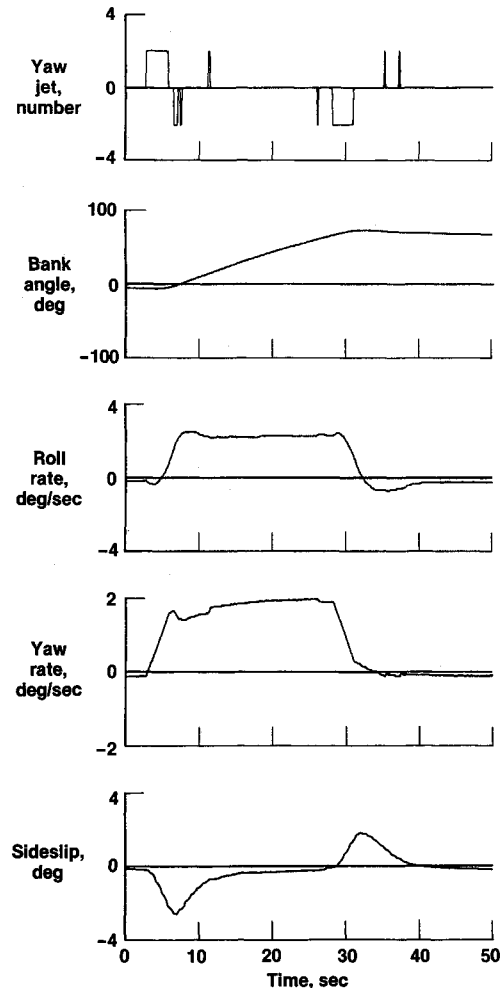


Fig. 20 Manual bank maneuver at $M = 24$ from STS-2.

and the basic control system remained unchanged. Since the response variables were kept low, and the inputs were slower and smaller, the flight responses on STS-2 to STS-4 did not show a tendency to oscillate. The software was updated for STS-5, and the resulting automated maneuver is essentially indistinguishable from that shown in Fig. 20. This maneuver has been used on all subsequent Shuttle flights.

The application of parameter estimation techniques to the highly complex Space Shuttle vehicle will continue, and the results of this application have and will significantly affect the control system design, placard modification, and flight procedures in general.

Concluding Remarks

In this paper, the aircraft parameter estimation problem is used as an example of how parameter estimation can be applied in many scientific and engineering fields to assess phenomenology from observations, and a brief survey of the literature is presented. The theory, a simple simulated example, and the application of experimental results to solve real problems, are given and explained. The maximum-likelihood parameter estimation technique was used in the F-14 program to effect control system changes that improved handling qualities at high angles of attack. Space Shuttle energy-management maneuvers have been redefined based on simulations using flight-determined stability and control estimates. Moreover, parameter estimation techniques are being relied on for future control system design, placard modification or removal, and flight procedures in general for the Space Shuttle.

The explanation of parameter estimation techniques and the demonstration of their highly successful application to the

aircraft problems are intended to inform and to encourage scientists in other fields to consider these techniques for application to problems where a representative model and high-quality data exist.

References

- ¹Iliff, K. W. and Maine, R. E., "NASA Dryden's Experience in Parameter Estimation and Its Use in Flight Test," AIAA Paper 82-1373, Aug. 1982.
- ²Iliff, K. W. and Maine, R. E., "More Than You May Want to Know About Maximum-Likelihood Estimation," NASA TM-85905, 1985.
- ³Zadeh, L. A. and Desoer, C. A., *Linear System Theory*, McGraw-Hill, New York, 1963.
- ⁴Schweppe, F. C., *Uncertain Dynamic Systems*, Prentice-Hall, Englewood Cliffs, NJ, 1973.
- ⁵Maine, R. E. and Iliff, K. W., "Identification of Dynamic Systems," AGARD-AG-300, 1984; also, NASA RP-1138, 1985.
- ⁶Maine, R. E. and Iliff, K. W., "Application of Parameter Estimation to Aircraft Stability and Control—The Output-Error Approach," NASA RP-1168, 1986.
- ⁷Norton, F. H., "The Measurement of the Damping in Roll on a JN4h in Flight," NACA Rept. 167, 1923.
- ⁸Norton, F. H., "A Study of Longitudinal Dynamic Stability in Flight," NACA Rept. 170, 1923.
- ⁹Iliff, K. W. and Maine, R. E., "A Bibliography for Aircraft Parameter Estimation," NASA TM-86804, 1986.
- ¹⁰Gauss, K. F., *Theory of the Motion of the Heavenly Bodies Moving About the Sun in Conic Sections*, translated from *Theoria Motus*, 1809, by Charles Henry Davis, 1857, Dover, New York, 1847.
- ¹¹Douglas, J., "Theorems in the Inverse Problem in the Calculus of Variations," *Proceedings of the National Academy of Science*, Vol. 16, No. 3, 1940.
- ¹²Gelfand, I. M. and Levitan, B. M., "On the Determination of a Differential Equation From Its Spectral Function," *Izvestiya Ak.*, Vol. 15, No. 4, Nauk, USSR, 1951.
- ¹³Feldbaum, A. A., "Dual Control Theory," *Automn. Remote Control*, Vol. 22, 1961, pp. 1-12, 109-121.
- ¹⁴Cuenod, M. and Sage, A., "Comparison of Some Methods Used for Process Identification," *Automatica*, Vol. 4, 1968, pp. 235-269.
- ¹⁵Balakrishnan, A. V. and Peterka, V., "Identification in Automatic Control Systems," *Automatica*, Vol. 5, 1969, pp. 817-829.
- ¹⁶Åström, K. J. and Eykhoff, P., "System Identification—A Survey," *Automatica*, Vol. 7, No. 2, 1971, pp. 123-162.
- ¹⁷Eykhoff, P., *System Identification, Parameter and State Estimation*, Wiley, London, 1974.
- ¹⁸Åström, K. J., "Control Problems in Papermaking," *Proceedings of the IBM Scientific Computing Symposium on Control Theory and Applications*, IBM Data Processing Div., White Plains, New York, 1966, pp. 135-167.
- ¹⁹Kashyap, R. L., "A New Method of Recursive Estimation in Discrete Linear Systems," *IEEE Transactions on Automatic Control*, Vol. AC-15, No. 1, Feb. 1970, pp. 18-24.
- ²⁰Balakrishnan, A. V., "Stochastic System Identification Techniques," *Stochastic Optimization and Control*, edited by H. F. Karman, Wiley, London, 1968.
- ²¹Balakrishnan, A. V., "Stochastic Differential System I," *Filtering and Control; A Function Space Approach*, Lecture Notes in Economics and Mathematical Systems, Vol. 84, edited by M. Beckman, G. Goos and H. P. Kunzi, Springer-Verlag, Berlin, 1973.
- ²²Balakrishnan, A. V., "Modelling and Identification Theory: A Flight Control Application," *Theory and Applications of Variable Structure Systems*, edited by R. B. Mohler and A. Ruberti, Academic, New York, 1972.
- ²³Iliff, K. W., "Identification and Stochastic Control with Application to Flight Control in Turbulence," Ph.D. Dissertation, Univ. of California, Los Angeles, CA, May 1973.
- ²⁴Maine, R. E. and Iliff, K. W., "The Theory and Practice of Estimating the Accuracy of Dynamic Flight-Determined Coefficients," NASA RP-1077, 1981.
- ²⁵"Parameter Estimation Techniques and Applications in Aircraft Flight Testing," NASA TN-D-7647, 1974.
- ²⁶"Methods for Aircraft State and Parameter Identification," AGARD-CP-172, May 1975.
- ²⁷Breuhäus, W. O., "Summary of Dynamic Stability and Control Flight Research Conducted Utilizing a B-25J Airplane," Cornell Aeronautical Lab., Buffalo, NY, Rept. TB-405-F-10, May 1948.
- ²⁸Seamans, R. C. Jr., Blasingame, B. P., and Clementson, G. C., "The Pulse Method for the Determination of Aircraft Dynamic Performance," *Journal of Aeronautical Science*, Vol. 17, No. 1, Jan. 1950, pp. 22-38.
- ²⁹Greenberg, H., "A Survey of Methods for Determining Stability Parameters of an Airplane From Dynamic Flight Measurements," NACA TN-2340, 1951.
- ³⁰Shinbrot, M., "On the Analysis of Linear and Nonlinear Dynamical Systems From Transient-Response Data," NACA TN-3288, 1954.
- ³¹Howard, J., "The Determination of Lateral Stability and Control Derivatives From Flight Data," *Can. Aeronautics Space J.*, Vol. 13, March 1967, pp. 126-134.
- ³²Wolowicz, C. H., "Considerations in the Determination of Stability and Control Derivatives and Dynamic Characteristics From Flight Data," AGARD-AR-549, Pt. 1, 1966.
- ³³Rampy, J. M. and Berry, D. T., "Determination of Stability Derivatives From Flight Test Data by Means of High Speed Repetitive Operation Analog Matching," FTC-TDR-64-8, Edwards, CA, May 1964.
- ³⁴Rynaski, E. G., "Application of Advanced Identification Techniques to Nonlinear Equations of Motion," *Proceedings of the Stall/Post-Stall/Spin Symposium*, Wright-Patterson AFB, OH, Dec. 1971, pp. 0-1 to 0-18.
- ³⁵Iliff, K. W. and Taylor, L. W. Jr., "Determination of Stability Derivatives From Flight Data Using a Newton-Raphson Minimization Technique," NASA TN-D-6579, 1972.
- ³⁶Taylor, L. W., Jr. and Iliff, K. W., "A Modified Newton-Raphson Method for Determining Stability Derivatives From Flight Data," *Second International Conference on Computing Methods in Optimization Problems*, Academic, New York, 1969, pp. 353-364.
- ³⁷Larson, D. B. and Fleck, J. T., "Identification of Parameters by the Method of Quasilinearization," Cornell Aeronautical Lab., Buffalo, NY, Rept. 164, May 1968.
- ³⁸Balakrishnan, A. V., *Communication Theory*, McGraw-Hill, New York, 1968.
- ³⁹Bellman, R. E. and Kalaba, R. E., *Quasilinearization and Nonlinear Boundary-Value Problems*, American Elsevier, New York, 1965.
- ⁴⁰Taylor, L. W. Jr., Iliff, K. W., and Powers, B. G., "A Comparison of Newton-Raphson and Other Methods for Determining Stability Derivatives From Flight Data," AIAA Paper 69-315, March 1969.
- ⁴¹Grove, R. D., Bowles, R. L., and Mayhew, S. C., "A Procedure for Estimating Stability and Control Parameters From Flight Test Data by Using Maximum Likelihood Methods Employing a Real-Time Digital System," NASA TN-D-6735, 1972.
- ⁴²Ross, A. J. and Foster, G. W., "FORTRAN Programs for the Determination of Aerodynamic Derivatives From Transient Longitudinal or Lateral Responses of Aircraft," Royal Aircraft Establishment, TR-75090, Sept. 1975.
- ⁴³Maine, R. E. and Iliff, K. W., "A FORTRAN Program for Determining Aircraft Stability and Control Derivatives From Flight Data," NASA TN-D-7831, 1975.
- ⁴⁴Nagy, C. J., "A New Method for Test and Analysis of Dynamic Stability and Control," Air Force Flight Test Center, Edwards, CA, AFFTC-TD-75-4, May 1976.
- ⁴⁵Iliff, K. W., Maine, R. E., and Shafer, M. F., "Subsonic Stability and Control Derivatives for an Unpowered, Remotely Piloted 3/8-scale F-15 Airplane Model Obtained From Flight Test," NASA TN-D-8136, 1976.
- ⁴⁶Sim, A. G., "A Correlation Between Flight-Determined Derivatives and Wind-Tunnel Data for the X-24B Research Aircraft," NASA SX-3371, 1976.
- ⁴⁷Jeglum, P. M., "AFFTC Experience in the Use of Flight-Test Derived Stability Derivatives," AGARD Fluid Dynamics Panel Symposium on Dynamic Stability Parameters, Athens, Greece, Paper 14, 1978.
- ⁴⁸Holleman, E. C., "Summary of Flight Tests to Determine the Spin and Controllability Characteristics of a Remotely Piloted, Large-Scale (3/8) Fighter Airplane Model," NASA TN-D-8052, 1976.
- ⁴⁹Smith, H. J., "Flight-Determined Stability and Control Derivatives for an Executive Jet Transport," NASA TM-X-56034, 1975.
- ⁵⁰Suit, W. T., "Aerodynamic Parameters of the Navion Airplane Extracted From Flight Data," NASA TN-D-6643, 1972.
- ⁵¹Frei, D. R., "Practical Applications of Parameter Identification," AIAA Paper 77-1136, Aug. 1977.
- ⁵²Ross, A. J., "Determination of Aerodynamic Derivatives From Transient Response in Manoeuvring Flight," *Methods for Aircraft State and Parameter Identification*, AGARD-CP-172, May 1975, pp. 14-1-14-10.
- ⁵³Gould, D. G., and Hindson, W. S., "Estimates of the Stability Derivatives of a Helicopter and a V/STOL Aircraft From Flight Data," *Methods for Aircraft State and Parameter Identification*,

AGARD-CP-172, May 1975, pp. 23-1-23-9.

⁵⁴Klein, V., "Longitudinal Aerodynamic Derivatives of a Slender Delta-Wing Research Aircraft Extracted From Flight Data," Cranfield Inst. of Technology, Cranfield, England, UK, CIT-FI-74-023, July 1974.

⁵⁵Schuetz, A. J., "Low Angle-of-Attack Longitudinal Aerodynamic Parameters of Navy T-2 Trainer Aircraft Extracted From Flight Data: A Comparison of Identification Technique. Volume I—Data Acquisition and Modified Newton-Raphson Analysis," Naval Air Development Center, Warminster, PA, NADC-74181-30-VOL-1 AD-A013181, June 1975.

⁵⁶Marchand, M. and Koehler, R., "Determination of Aircraft Derivatives by Automatic Parameter Adjustment and Frequency Response Methods," *Methods for Aircraft State and Parameter Identification*, AGARD-CP-172, May 1975, pp. 17-1-17-18.

⁵⁷"Dynamic Stability Parameters," AGARD-CP-235, 1978.

⁵⁸"Parameter Identification," AGARD-LS-104, 1979.

⁵⁹Mehra, R. K., "Maximum Likelihood Identification of Aircraft Parameters," *Proceedings of the Eleventh Joint Automatic Control Conference of the American Automatic Control Council*, Paper 18-C, June 1970, pp. 442-444.

⁶⁰Tyler, J. S., Powell, J. D., and Mehra, R. K., "The Use of Smoothing and Other Advanced Techniques for VTOL Aircraft Parameter Identification," Final Rept., Naval Air Systems Command Contract N00019-69-C-0534, Systems Control, Inc., Palo Alto, CA, June 1970.

⁶¹Gerlach, O. H., "The Determination of Stability Derivatives and Performance Characteristics From Dynamic Manoeuvres," Delft Univ. of Technology, Dept. of Aerospace Engineering, Delft, The Netherlands, Rept. VTH-163, March 1971.

⁶²Jonkers, H. L., "Application of the Kalman Filter to Flight Path Reconstruction From Flight Test Data Including Estimation of Instrumental Bias Error Corrections, Delft Univ. of Technology, Dept. of Aerospace Engineering, Delft, the Netherlands, Rept. VTH-162, Feb. 1976.

⁶³Chen, R. T. N. and Eulrich, B. J., "Parameter and Model Identification of Nonlinear Dynamical Systems Using a Suboptimal Fixed-Point Smoothing Algorithm," *Proceedings of the Twelfth Joint Automatic Control Conference of the American Automatic Control Council*, Paper 7-E2, Aug. 1971, pp. 731-740.

⁶⁴Yazawa, K., "Identification of Aircraft Stability and Control

Derivatives in the Presence of Turbulence," AIAA Paper 77-1134, Aug. 1977.

⁶⁵Iliff, K. W. and Maine, R. E., "Practical Aspects of Using a Maximum Likelihood Estimator," *Methods for Aircraft State and Parameter Identification*, AGARD-CP-172, Paper 16, May 1975, pp. 16-1-16-15.

⁶⁶Iliff, K. W. and Maine, R. E., "Further Observations on Maximum Likelihood Estimates of Stability and Control Characteristics Obtained From Flight Data," AIAA Paper 77-1133, Aug. 1977.

⁶⁷Maine, R. E. and Iliff, K. W., *User's Manual for MMLE3, A General FORTRAN Program for Maximum Likelihood Parameter Estimation*, NASA TP-1563, 1980.

⁶⁸Maine, R. E. and Iliff, K. W., "Formulation and Implementation of a Practical Algorithm for Parameter Estimation with Process and Measurement Noise," *SIAM Journal of Applied Mathematics*, Vol. 41, No. 3, Dec. 1981, pp. 558-579.

⁶⁹Nguyen, L. T., Gilbert, W. P., Gera, J., Iliff, K. W., and Enevoldson, E. K., "Application of High-Alpha Control System Concepts to a Variable-Sweep Fighter Airplane," AIAA Paper 80-1582, Aug. 1980.

⁷⁰Gera, J., Wilson, R. J., and Enevoldson, E. K., "Flight Test Experience With High- α Control System Techniques on the F-14 Airplane," AIAA Paper 81-2505, Nov. 1981.

⁷¹Gera, J., "Simulation as an Analysis Tool in Flight Testing a Modified Control System on the F-14 Airplane," *SES/SFTE Simulation-Aircraft Test and Evaluation Symposium*, Patuxent River, MD, March 1982.

⁷²Cooke, D. R., "Space Shuttle Stability and Control Flight Test Techniques," AIAA Paper 80-1608, Aug. 1980.

⁷³Young, J. C. and Underwood, J. M., "The Development of Aerodynamic Uncertainties for the Space Shuttle Orbiter," AIAA Paper 82-0563, March 1982.

⁷⁴Weil, J. and Powers, B. G., "Correlation of Predicted and Flight Derived Stability and Control Derivatives—With Particular Application to Tailless Delta Wing Configurations," NASA TM-81361, 1981.

⁷⁵Iliff, K. W., Maine, R. E., and Cooke, D. R., "Selected Stability and Control Derivatives From the First Space Shuttle Entry," AIAA Paper 81-2451, Nov. 1981.

⁷⁶Maine, R. E. and Iliff, K. W., "Selected Stability and Control Derivatives from the First Three Space Shuttle Entries," AIAA Paper 81-1318, Aug. 1982.

Recommended Reading from the AIAA Progress in Astronautics and Aeronautics Series . . .



Monitoring Earth's Ocean, Land and Atmosphere from Space: Sensors, Systems, and Applications

Abraham Schnapf, editor

This comprehensive survey presents previously unpublished material on past, present, and future remote-sensing projects throughout the world. Chapters examine technical and other aspects of seminal satellite projects, such as Tiros/NOAA, NIMBUS, DMS, LANDSAT, Seasat, TOPEX, and GEOSAT, and remote-sensing programs from other countries. The book offers analysis of future NOAA requirements, spaceborne active laser sensors, and multidisciplinary Earth observation from space platforms.

TO ORDER: Write AIAA Order Department,
370 L'Enfant Promenade, S.W., Washington, DC 20024

Please include postage and handling fee of \$4.50 with all orders.
California and D.C. residents must add 6% sales tax. All foreign orders
must be prepaid. Please allow 4-6 weeks for delivery. Prices are subject
to change without notice.

1985 830 pp., illus. Hardback

ISBN 0-915928-98-1

AIAA Members \$59.95

Nonmembers \$99.95

Order Number V-97